

Split Instability of a Vortex in an Attractive Bose-Einstein Condensate

Hiroki Saito and Masahito Ueda

Department of Physics, Tokyo Institute of Technology, Tokyo 152-8551, Japan

(Dated: December 2, 2024)

An attractive Bose-Einstein condensate with a vortex in isotropic or oblate traps is found to split into two pieces via the quadrupole instability, which arises at a weaker strength of interaction than the monopole and the dipole instabilities. The split pieces subsequently unite to recover the original vortex or collapse.

PACS numbers: 03.75.Fi, 05.30.Jp, 32.80.Pj, 67.40.Vs

Quantized vortices in gaseous Bose-Einstein condensates (BECs) offer a visible hallmark of superfluidity [1, 2, 3], where repulsive interatomic interactions play a crucial role in the vortex stabilization and lattice formation. Attractive BECs, on the other hand, cannot hold vortices in any thermodynamically stable state [4, 5, 6]. However, owing to the recent development of the Feshbach technique [7], by which the strength and the sign of interactions can be controlled [8, 9, 10], we can prepare a vortex in an attractive BEC by creating a vortex in a repulsive BEC and then switching the sign of interaction to attractive. The ensuing dynamics of this system reveals previously unknown dynamical instabilities, which we would like to address in this Letter.

Suppose that a singly quantized vortex is created in a BEC with repulsive interaction and that the strength of interaction is adiabatically changed from repulsive to attractive. According to previous work [11, 12] the vortex state remains metastable until the strength of the interaction g reaches a critical value g_M^{cr} , and when $|g|$ exceeds $|g_M^{\text{cr}}|$, the system develops a monopole (breathing-mode) instability and collapses. This conclusion holds if the system has the exact axisymmetry. In practice, however, the system is always subject to external disturbances such as those brought by the stirring laser beam that break the exact axisymmetry. We note that a single vortex observed by the ENS group [2] would not have been created if the system had maintained the exact axisymmetry. In this Letter we show that even an infinitesimal symmetry-breaking perturbation induces the dynamical quadrupole instability that appears for $|g|$ smaller than $|g_M^{\text{cr}}|$. This instability causes the BEC to split into two pieces that rotate around the center of the trap. Surprisingly, in some parameter regime, these pieces subsequently unite to recover the original vortex, and this split-merge cycle repeats. Below we report the results of our studies on this novel phenomenon.

We first investigate the Bogoliubov excitation spectrum of the single-vortex state. This state minimizes the Gross-Pitaevskii (GP) energy functional within the functional space $\psi_0 = f(r)e^{i\phi}$ with $r = (x^2 + y^2)^{1/2}$, and

is the stationary solution of the GP equation

$$i\frac{\partial\psi}{\partial t} = \left[-\frac{1}{2}\nabla^2 + \frac{1}{2}(r^2 + \lambda^2 z^2) + g|\psi|^2 \right] \psi, \quad (1)$$

where the length, time, and ψ are normalized in units of $d_0 \equiv (\hbar/m\omega_\perp)^{1/2}$, ω_\perp^{-1} , and $(N/d_0^3)^{1/2}$, respectively. Here ω_\perp is the radial trap frequency, N the number of BEC atoms, and $\lambda \equiv \omega_z/\omega_\perp$ the asymmetry parameter of an axisymmetric trap. In Eq. (1), $g \equiv 4\pi Na/d_0$ characterizes the strength of interaction, where a is the s-wave scattering length. The excitation spectrum in a rotating frame is obtained by diagonalizing the Bogoliubov-de Gennes equations

$$(K_0 - \Omega L_z + 2g|\psi_0|^2) u_n + g\psi_0^2 v_n = E_n u_n, \quad (2a)$$

$$(K_0 + \Omega L_z + 2g|\psi_0|^2) v_n + g\psi_0^{*2} u_n = -E_n v_n, \quad (2b)$$

where $K_0 \equiv -\nabla^2/2 + (r^2 + \lambda^2 z^2)/2 - \mu$, and n is the index of the eigenmode. The angular velocity Ω of the external rotation is normalized by ω_\perp , and $L_z \equiv -i\partial/\partial\phi$. For a vortex state $\psi_0 \propto e^{i\phi}$, each angular momentum state $u_n \propto e^{im\phi}$ is coupled only to $v_n \propto e^{i(m-2)\phi}$, and we shall refer to m as the angular momentum of the excitation.

We follow Ref. [13] to numerically analyze Eqs. (2) and find that there is at least one negative eigenvalue in the $m = 0$ mode for any $g < 0$, $|\Omega| < 1$, and λ . We have also confirmed that the energy of the vortex state ψ_0 is always larger than that of the non-vortex ground state. The vortex state with attractive interactions is therefore thermodynamically unstable as has been shown in the quasi-1D toroidal trap [4, 5, 6], and is fragile against environmental disturbances. The vortex is thus likely to spiral out from the condensate, and the state will eventually relax to the non-vortex ground state by dissipating its energy and angular momentum. At sufficiently low temperature in a high-vacuum chamber, however, the thermodynamical instability is irrelevant, since the energy and angular momentum are conserved. In fact, recent experiments [2] have demonstrated that in spite of the thermodynamical instability, the vortex state in a stationary trap has the lifetime of ~ 1 s, which is much longer than the characteristic time scale of the dynamics that we discuss below.

When the complex eigenvalues emerge in the Bogoliubov spectrum, the amplitude of the corresponding mode

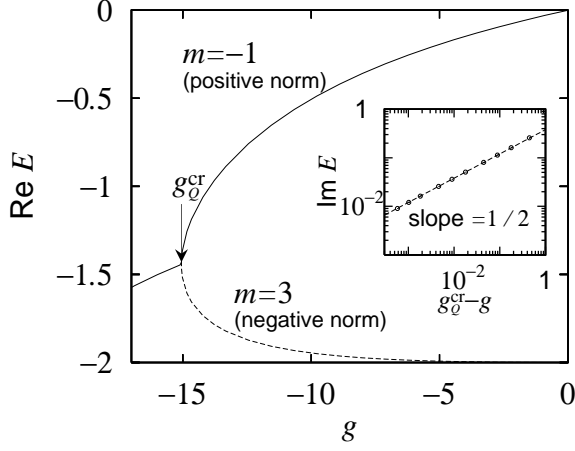


FIG. 1: For $g > g_Q^{\text{cr}} = -15.06$ the solid curve denotes the eigenvalue (real) of the $m = -1$ mode, and the dashed one that of the negative-norm branch of the $m = 3$ mode in an isotropic trap. These two branches merge at $g = g_Q^{\text{cr}}$ below which the eigenvalue becomes complex and the dynamical instability appears. Inset: the circles show the imaginary part of the complex eigenvalues for $g < g_Q^{\text{cr}}$, and the dashed line is proportional to $\sqrt{g_Q^{\text{cr}} - g}$.

grows exponentially in time. As noise is inevitable in experimental situations, such *dynamical instabilities* are more important than the thermodynamical one at low temperature.

Figure 1 shows the real and imaginary parts of the lowest eigenvalues of the $m = -1$ and 3 excitations in an isotropic trap. The eigenvalues become complex at the critical strength of interaction $g_Q^{\text{cr}} = -15.06$, showing the onset of the dynamical instability in the quadrupole mode. The imaginary part of the complex eigenvalue is proportional to $\sqrt{g_Q^{\text{cr}} - g}$ as shown in the inset in Fig. 1. The complex eigenvalues emerge also in the dipole modes, i.e., $m = 0$ and 2, at $g_D^{\text{cr}} = -18.02$, whose g -dependence is similar to that in Fig. 1. The eigenvalues with other m are real for g larger than the critical value for the monopole (radial-breathing-mode) instability $g_M^{\text{cr}} = -23.7$.

Figure 2 shows the λ dependence of g_Q^{cr} , g_D^{cr} , g_M^{cr} , and $g_{\text{nonvortex}}^{\text{cr}}$ in axi-symmetric traps, where $g_{\text{nonvortex}}^{\text{cr}}$ is the critical value for the non-vortex state to collapse through the monopole instability. We note that g_M^{cr} is always smaller than g_Q^{cr} and g_D^{cr} , and hence the latter instabilities arise before the monopole instability sets in. For a trap with $\lambda \gtrsim 0.3$, the quadrupole instability arises before the dipole one unlike the quasi-1D toroidal trap [4, 5, 6].

We performed numerical diagonalization also for 2D systems. Strong confinement in the z direction realizes the quasi-2D trap, when $\hbar\omega_z$ is much larger than the characteristic energy of the dynamics, and the effective interaction strength in the quasi-2D oblate trap is given by $g^{2D} = \sqrt{\lambda/(2\pi)}g^{3D}$ [14]. In the 2D system, the dy-

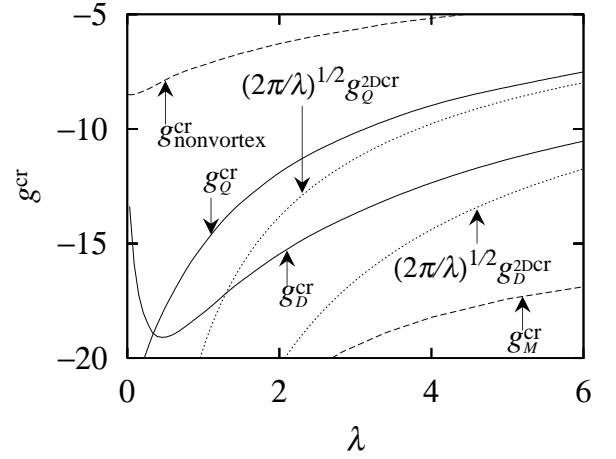


FIG. 2: The $\lambda \equiv \omega_z/\omega_\perp$ dependence of the critical strength of interaction for the quadrupole mode g_Q^{cr} and the dipole mode g_D^{cr} (solid curves) above the single-vortex state. The critical values for the monopole mode g_M^{cr} above the vortex state and that above the non-vortex ground state $g_{\text{nonvortex}}^{\text{cr}}$ are plotted with the dashed curves. The two dotted curves are $(2\pi/\lambda)^{1/2}g_Q^{2\text{Dcr}}$ and $(2\pi/\lambda)^{1/2}g_D^{2\text{Dcr}}$.

namical instability arises in the quadrupole and dipole modes at $g_Q^{2\text{Dcr}} = -7.79$ and $g_D^{2\text{Dcr}} = -11.48$, respectively. The dependencies of the complex eigenvalues on g are similar to that in Fig. 1. As shown in Fig. 2, the critical values in 3D approach $\sqrt{2\pi/\lambda}$ times as large as those in 2D as λ increases.

To understand the dynamical instabilities described above, let us consider the GP action integral in 2D

$$S = \int dt \int d\mathbf{r} \psi^* \left(-i \frac{\partial}{\partial t} - \frac{\nabla^2}{2} + \frac{r^2}{2} + \frac{g}{2} |\psi|^2 \right) \psi. \quad (3)$$

We assume that the state evolution is described by $\psi = \sum_m c_m(t) \phi_m(\mathbf{r})$, where $\phi_m(\mathbf{r})$ is assumed to take the form of $\phi_m(\mathbf{r}) = [r^{|m|}/(\sqrt{\pi}|m|!d^{|m|+1})] \exp[-r^2/(2d^2) + im\phi]$ and $d = [1 + g/(8\pi)]^{1/4}$ minimizes the GP energy functional for the $m = 1$ state. Substituting this ψ into Eq. (3) and minimizing S with respect to c_m yields

$$i\dot{c}_m = \varepsilon_m c_m + g \sum_{mm_1m_2m_3} G_{m_2,m_3}^{m,m_1} c_{m_1}^* c_{m_2} c_{m_3}, \quad (4)$$

where $\varepsilon_m \equiv \int d\mathbf{r} (|\nabla\psi_m|^2 + r^2|\psi_m|^2)/2$ and $G_{m_3,m_4}^{m_1,m_2} \equiv \int d\mathbf{r} \psi_{m_1}^* \psi_{m_2}^* \psi_{m_3} \psi_{m_4}$. When the BEC exists in the $m = 1$ mode, we obtain $c_1(t) = e^{-i\mu t} + O(|c_{m \neq 1}|^2)$ with $\mu = 1/d^2 + d^2 + g/(4\pi d^2)$. The linear analysis of Eq. (4) for $\tilde{c}_m \equiv e^{i\mu t} c_m$ ($m \neq 1$) yields

$$i\dot{\tilde{c}}_m = (\varepsilon_m - \mu)\tilde{c}_m + 2G_{m,1}^{m,1}\tilde{c}_m + G_{1,1}^{m,2-m}\tilde{c}_{2-m}^*. \quad (5)$$

It follows from this that for $m = -1$ the eigenfrequencies are given by $A \pm \sqrt{B}$, where $A \equiv [g/(8\pi) - 1]/[1 + g/(8\pi)]^{1/2}$ and $B \equiv 3 + 5g/(8\pi) + [1 + g/(2\pi) -$

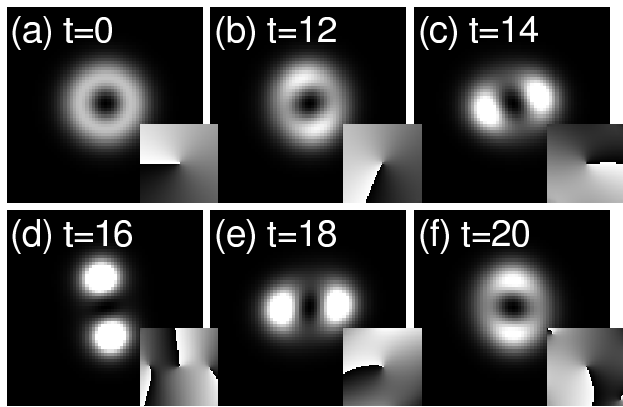


FIG. 3: The density and phase (insets) profiles of the time evolution of the vortex state with $g = -9$. The initial state is the stationary solution of the Gross-Pitaevskii equation plus small perturbation. The gray scale in the insets indicates the phase from $(2n-1)\pi$ to $(2n+1)\pi$ with an integer n . The sizes of the figures and insets are 10×10 in unit of $(\hbar/m\omega_{\perp})^{1/2}$.

$g^2/(32\pi^2)]/[1 + g/(8\pi)]$. We find that B is a monotonically increasing function for $g > -8\pi$, and B becomes negative for $g > g^{\text{cr}} \simeq -9.2$, which is in reasonable agreement with $g_Q^{2\text{Dcr}} = -7.79$ stated above. We also find that the imaginary part appearing for $g < g^{\text{cr}}$ is proportional to $\sqrt{g^{\text{cr}} - g}$, in agreement with the inset of Fig. 1.

The Bogoliubov analysis discussed above is valid only if deviations from the initial state are small. To follow further evolution of the wave function we must solve the time-dependent GP equation (1). Since we study the growth of small perturbation, high precision is required in the numerical integration, and hence we consider the 2D model to ensure sufficiently small discretization in the Crank-Nicholson scheme [15]. This situation corresponds to the oblate trap with large λ .

Figure 3 shows time evolution of the density and phase profiles with $g = -9$, which exceeds the critical value for the quadrupole mode $g_Q^{2\text{Dcr}} = -7.79$ but does not exceed that for the dipole mode $g_D^{2\text{Dcr}}$. A small perturbation is added to the initial state to imitate noise in realistic situations. Due to the quadrupole instability, the vortex is first stretched [Fig. 3 (b)], and then splits into two clusters that rotate around the center of the trap [Fig. 3 (d)] with angular velocity $\Omega \simeq 0.73$. The $m = -1$ and 3 components grow exponentially, and their Lyapunov exponents agree with the imaginary part of the complex eigenvalues. Interestingly, the split process is reversible: the two clusters subsequently unite to recover the ring shape [Fig. 3 (f)], and this split-merge processes repeat. We numerically checked that no split-merge phenomenon occurs for $g > g_Q^{2\text{Dcr}}$.

The insets in Fig. 3 show the phase plots. At $t = 16$, there are three topological defects: the central one exists from the start, and the other two enter as the vortex splits, in accordance with the fact that the $m = 3$ compo-

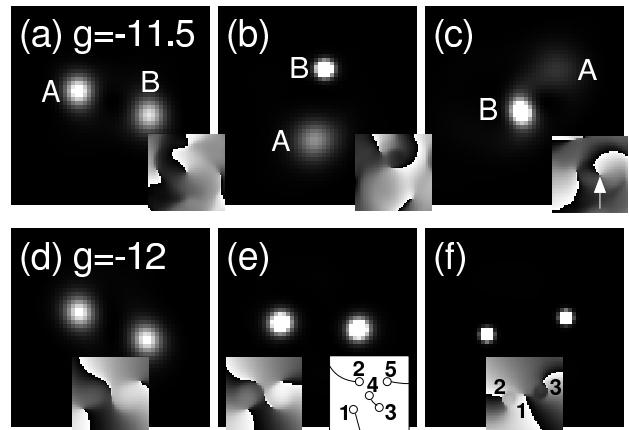


FIG. 4: The density and phase (insets) plots of the time evolution after the vortex split with $g = -11.5$ in (a)-(c) and with $g = -12$ in (d)-(f). The time interval between each image is $\Delta t = 2$ in (a)-(c) and $\Delta t = 0.4$ in (d)-(f). The right inset in (e) illustrates the topological defects and branch cuts in the left one. The sizes of the images are 8×8 in unit of $(\hbar/m\omega_{\perp})^{1/2}$. The sensitivity of imaging of the density plots is $1/4$ of that in Fig. 3.

nent grows upon the vortex split. The two side vortices cannot be seen in the density plot, and hence they may be called “ghost” vortices [16], which carry the angular momentum very little.

When $|g|$ exceeds $|g_D^{2\text{Dcr}}| = 11.48$, the dipole instability arises in addition to the quadrupole one. The dipole instability plays the role of transferring atoms from one to the other of the two clusters, thereby inducing the collapse. Figures 4 (a)-(c) show the collapse process with $g = -11.5$. After the split-merge process repeats a few times, the balance between the two clusters is broken due to the dipole instability. The cluster labeled A first grows [Fig. 4 (a)], then B grows [Fig. 4 (b)] like seesaw, and eventually B absorbs A and collapses [Fig. 4 (c)], where the original topological defect begins to spiral out as indicated by the white arrow in the inset. In the case with $g = -12$, both clusters collapse immediately after the vortex split as shown in Figs. 4 (d)-(f). In this collapse process, we found the exchange of a vortex-antivortex pair as follows. In the insets of Fig. 4 (e), where the right one illustrates the topological defects and branch cuts in the left, the end part of the branch cut of the central vortex is separated off to create two vortices with opposite circulations (labeled 3 and 4). The vortices 4 and 5 then merge, and the vortex 1 comes to the center [inset of Fig. 4 (f)], where the other two vortices (2 and 3) are attracted to the clusters. This phenomenon is seen also in the course of the split-merge process with $g = -11.5$, while it is not seen when the attractive interaction is weak, say, at $g = -9$.

When the size of the system becomes too small due to the attractive interaction to observe by the *in situ*

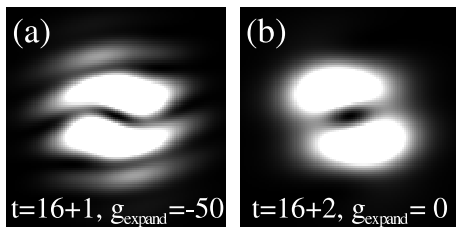


FIG. 5: (a) The density plot at $t = 17$, where the interaction is switched from $g = -9$ to $g_{\text{expand}} = -50$ and the trap is switched off at $t = 16$ in Fig. 3. (b) The density plot at $t = 18$ with $g_{\text{expand}} = 0$. The sizes of the images are 25×25 in unit of $(\hbar/m\omega_{\perp})^{1/2}$. The sensitivity of imaging is 20 times larger than that in Fig. 3.

imaging method, the condensate must be expanded before imaging. Figure 5 (a) shows the expanded image at $t = 17$, where the interaction is switched from $g = -9$ to $g_{\text{expand}} = 50$ and the trapping potential is switched off at $t = 16$ [Fig. 3 (d)]. The image shows the interference fringes due to the overlap of the atomic clouds expanded from the two clusters. The wavelength of the interference pattern is proportional to the expansion time. The destructive interference line occurs at the center, since the phases of the two clusters differ by π . Figure 5 (b) shows the expanded image at $t = 18$ with $g_{\text{expand}} = 0$. Comparing Figs. 5 (a) and (b), we find that the repulsive interaction makes more fringes and bends them around the center.

The split instability shown above should be distinguished from the structural instability in Ref. [17], which arises from the trap asymmetry in the radial directions. In a realistic axisymmetric trap, the time for the structural instability to appear is much larger than that of the split instability, and therefore the latter is dominant.

Our stability analysis presented above is restricted to the region where the mean-field theory well describes the system, i.e., $|a|/d_0 \ll 1$ and $N \gg 1$. In the region where the mean-field theory breaks down, the rotating states are always unstable in quasi-1D [6], suggesting that the instability of the vortex state in a 3D trap is enhanced when the quantum fluctuations become significant. The stability analysis in this region requires us to go beyond the mean-field theory, and merits further study.

Finally, we comment on what happens when the interaction is switched to a large attractive value $g \ll g_M^{\text{cr}}$. As the condensate gradually shrinks, the shell structure in atomic density is formed, and the shells go towards the center of the trap due to the attractive interactions. Unlike the non-vortex cases [18], however, the atoms cannot collapse at the center because of the topological defect. Instead, each shell splits into several parts due to multipole instabilities, and the fragments collapse and explode [10], leading to the very complicated dynamics.

In conclusion, we have studied the stability properties of the vortex state with attractive interactions, and found

the dynamical instabilities that break the axisymmetry. This arises before g reaches the critical strength of interaction of the radial-collapsing instability g_M^{cr} , namely, the vortex is revealed to be more unstable when the azimuthal dynamics is taken into account. The dynamical quadrupole instability splits the vortex into two clusters that rotate around the center of the trap. The two clusters unite to recover the vortex ring or eventually collapse. Such instabilities suggest that the single or multiple vortex state splits into multiple clusters in the collapse, each of which implodes and explodes. In other words, the rotating condensate collapses via the dynamical instabilities around its topological defects.

This work was supported by a Grant-in-Aid for Scientific Research (Grant No. 11216204) by the Ministry of Education, Science, Sports, and Culture of Japan, and by the Toray Science Foundation.

-
- [1] M. R. Matthews, B. P. Anderson, P. C. Haljan, D. S. Hall, C. E. Wieman, and E. A. Cornell, *Phys. Rev. Lett.* **83**, 2498 (1999).
 - [2] K. W. Madison, F. Chevy, W. Wohlleben, and J. Dalibard, *Phys. Rev. Lett.* **84**, 806 (2000).
 - [3] J. R. Abo-Shaeer, C. Raman, J. M. Vogels, and W. Ketterle, *Science* **292**, 476 (2001).
 - [4] D. S. Rokhsar, cond-mat/9709212.
 - [5] M. Ueda and A. J. Leggett, *Phys. Rev. Lett.* **83**, 1489 (1999).
 - [6] G. P. Berman, A. Smerzi, and A. R. Bishop, *Phys. Rev. Lett.* **88**, 120402 (2002).
 - [7] S. Inouye, M. R. Andrews, J. Stenger, H. -J. Miesner, D. M. Stamper-Kurn, and W. Ketterle, *Nature* **392**, 151 (1998).
 - [8] S. L. Cornish, N. R. Claussen, J. L. Roberts, E. A. Cornell, and C. E. Wieman, *Phys. Rev. Lett.* **85**, 1795 (2000).
 - [9] J. L. Roberts, N. R. Claussen, S. L. Cornish, E. A. Donley, E. A. Cornell, and C. E. Wieman, *Phys. Rev. Lett.* **86**, 4211 (2001).
 - [10] E. A. Donley, N. R. Claussen, S. L. Cornish, J. L. Roberts, E. A. Cornell, and C. E. Wieman, *Nature* **412**, 295 (2001).
 - [11] F. Dalfovo and S. Stringari, *Phys. Rev. A* **53**, 2477 (1996).
 - [12] S. K. Adhikari, *Phys. Rev. E* **65**, 016703 (2001).
 - [13] M. Edwards, R. J. Dodd, C. W. Clark, and K. Burnett, *J. Res. Natl. Inst. Stand. Technol.* **101**, 553 (1996).
 - [14] Y. Castin and R. Dum, *Eur. Phys. J. D* **7**, 399 (1999).
 - [15] P. A. Ruprecht, M. J. Holland, K. Burnett, and M. Edwards, *Phys. Rev. A* **51**, 4704 (1995).
 - [16] M. Tsubota, K. Kasamatsu, and M. Ueda, *Phys. Rev. A* **65**, 023603 (2002).
 - [17] J. J. García-Ripoll, G. Molina-Terriza, V. M. Pérez-García, and L. Torner, *Phys. Rev. Lett.* **87**, 140403 (2001).
 - [18] H. Saito and M. Ueda, *Phys. Rev. Lett.* **86**, 1406 (2001); *Phys. Rev. A* **63**, 043601 (2001); **65**, 033624 (2002).